Fabrication and characterization of high-resolution 4H-SiC epitaxial radiation detectors for challenging reactor dosimetry environments

Krishna C. Mandal[1], *Sandeep K.* Chaudhuri[1], *and Frank H.* Ruddy[2,*]

[1]Department of Electrical Engineering, University of South Carolina, Columbia, SC 29208, USA
[2]Ruddy Consulting, 2162 Country Manor Dr., Mount Pleasant, SC 28466, USA

Abstract. Reactor dosimetry environments require radiation detectors that are capable of operating at high temperatures in extremely high neutron and gamma-ray dose rates. Silicon carbide (SiC) is one of the most promising wide bandgap semiconductors (3.27 eV) for harsh environment applications due to its radiation hardness, high breakdown voltage, high electron saturation velocity, and high thermal conductivity. In this paper, we summarize the prospect of Schottky barrier radiation detectors, fabricated on highly crystalline low-defect detector-grade n-type 4H-SiC epitaxial layers with thickness ranging from 20 to 250 μm, for harsh environment applications. A comprehensive discussion on the characterization of the parameters that influence the energy resolution has been included. The usage of electrical and radiation spectroscopic measurements for characterizing the junction and rectification properties, minority carrier diffusion lengths, and energy resolution has been elaborated. Characterization of crucial factors that limit the energy resolution of the detectors such as charge trap centers using thermally stimulated transient techniques is summarized. Finally, the effect of neutron fluence on the performance of the 4H-SiC detectors is discussed.

1 Introduction

The advantages of nuclear power generation outweigh any renewable or non-renewable sources by a substantial margin provided the safety of nuclear reactors are assessed regularly, if not continuously [1] [2]. For example, reactor pressure vessels (RPV) in nuclear reactors are subjected to continuous bombardment by radiation from fission reactions of the nuclear fuel. Fast neutrons and, to a lesser extent, high energy gamma rays are primary causes of radiation damage as they cause embrittlement of the reactor vessel material with prolonged exposure and, hence, can lead to deterioration of the structural integrity of RPVs [3]. Standard safety measures comprise monitoring the damage in representative steel (RPV material) specimens and the corresponding neutron/gamma dose using dosimetry. The detectors used for neutron dosimetry must be capable of withstanding the harsh reactor environment i.e., high radiation doses and elevated temperatures. When it comes to radiation detection and

* Corresponding author: frankhruddy@gmail.com

© The Authors, published by EDP Sciences. This is an open access article distributed under the terms of the Creative Commons Attribution License 4.0 (http://creativecommons.org/licenses/by/4.0/).

measurements, semiconductor detectors have many advantages because of their compactness, fast and direct readout, high efficiency, and high resolution. However, most of the matured semiconductor detector technologies like silicon or germanium are not suitable for prolonged use in harsh environments due to their lower bandgaps and displacement thresholds. Lower bandgap causes high leakage currents even at room temperature and lower displacement threshold implies formation of a higher number of radiation-induced defects at lower energies. The 4H polytype of silicon carbide is a wide bandgap (3.27 eV at 300K) semiconductor that is extremely radiation hard due to the high displacement threshold of Si and C in the 4H-SiC lattice [4]. The thermal conductivity of 4H-SiC is also very high and its physical properties barely change with increased temperature. A 4H-SiC based JFET has been demonstrated to work continuously for prolonged periods at an operating temperature of 800 – 1000 ºC [5] [6]. The last decade has seen tremendous improvement in the growth technology to produce highly crystalline 4H-SiC epitaxial layers using chemical vapor deposition. These layers demonstrate excellent charge transport properties and yet cost much less to produce than single crystalline electronic-grade diamond [7]. Silicon carbide is also known for its physical strength, and it is also not prone to chemical corrosion. Being a wide bandgap semiconductor, 4H-SiC is insensitive to visible light and does not require light-tight encapsulation for most applications. Also, 4H-SiC is the only wide bandgap semiconductor whose native oxide is SiO_2, making it compatible with the matured silicon device fabrication technology. The unique combination of the above properties makes 4H-SiC the ideal and future material for electronic devices in harsh environments [8]. 4H-SiC epitaxial layers have been demonstrated as versatile high-resolution radiation detectors which are equally capable of detecting energetic charged particles as well as penetrating radiation such as neutrons and gamma rays [9] [10] [11] [12] [13] [14]. Fabrication of detectors for penetrating radiations has gained even more momentum recently with the advent of detector-grade thick (up to 250 μm) epitaxial layers [15] [16] [17]. In this article we discuss developments in the fabrication of state-of-the-art SiC Schottky barrier detectors (SBD) for harsh-environment applications and the techniques that predict their operation under such conditions through various material and device characterization techniques. The effect of fast-neutron bombardment on these radiation detectors is also discussed.

2 SiC epilayer growth and device fabrication

Growth of high-quality 4H-SiC epitaxial layers with a high degree of crystallinity is usually achieved through hot-wall chemical vapor deposition (CVD) [18]. The epitaxial layers discussed in this article are grown by hot wall CVD using dichlorosilane (SiH_2Cl_2) and propane (C_3H_8) as the precursors and hydrogen as the carrier gas. Unintentional doping of nitrogen impurity atoms results in n-type conductivity of the epilayers. The key factors to maintain during the growth are the carbon-to-silicon ratio which is necessary to control the formation of native point defects such as carbon/silicon vacancy/interstitials and other defect complexes, such as carbon antisite vacancy (CAV) pairs, as well as the growth rate which determines the uniformity of the crystalline nature of the epilayers. While impurity type defects such as titanium are mostly shallow levels, intrinsic deep level trap centers such as carbon vacancies pose serious threats as charges trapped in deep levels are prone to recombination leading to loss of signal and degradation of detector performance [4]. Apart from point defects, extended structural defects such as threading screw dislocations (TSD), threading edge dislocations (TED), and basal plane dislocations (BPD) also affect the crystallinity of the epilayers [19]. While TEDs are considered benign, micropipe defects (MPD), which are a type of TSDs, form high leakage current paths. The epilayers used in this study showed the presence of MPDs in areal concentrations less than 1 cm^{-2}. This low density enables the fabrication of detectors with entrance windows having large surface areas,

because of the low probability of subtending a defect. To prevent the formation of extended defects and their propagation from the substrate to the epilayer during the growth, off-axis, step-controlled growth techniques are adopted, and thin buffer layers are included. The present epilayers, with thickness ranging between 20-250 μm, are grown on the (0001) plane (Si face) of highly conducting n-type 350-μm thick substrates, 8° offcut towards the $\langle 11\bar{2}0\rangle$ direction. A 1 μm thick buffer epilayer with a nitrogen doping concentration of 1×10^{18} cm^{-3} has been included between the bulk substrate and the epilayer. Fig. 1(a) shows a schematic diagram of the various crystal planes and Fig. 1(b) shows the epilayer structure. The epilayers grown on 100 mm diameter substrates are diced in 8 mm × 8 mm square specimens for detector fabrication. The wafers are cleaned thoroughly using a Radio Corporation of America (RCA) cleaning method which removes organic and metallic contaminants [20]. The wafers are treated with 50% diluted hydrofluoric acid for 30 secs to remove the native SiO_2 layer.

To form the Schottky barrier junction, which also acts as the detector entrance window, a nickel layer with thickness less than 20 nm is deposited on the epilayer through sputter coating. Such thin contacts form transparent windows for most radiations [21]. The detectors used in this study have circular nickel contacts with an area of 11 mm^2. A thicker (≈100 nm) nickel contact is deposited on the bulk side to form the Ohmic cathode. The detectors are generally mounted on printed circuit boards (PCB) using conductive epoxy on the cathode side and wire bonded on the anode for radiation detection measurements, However, for several other measurements spring loaded removable contact probes have been used. Fig. 1(c) shows a typical 4H-SiC SBD mounted on a PCB.

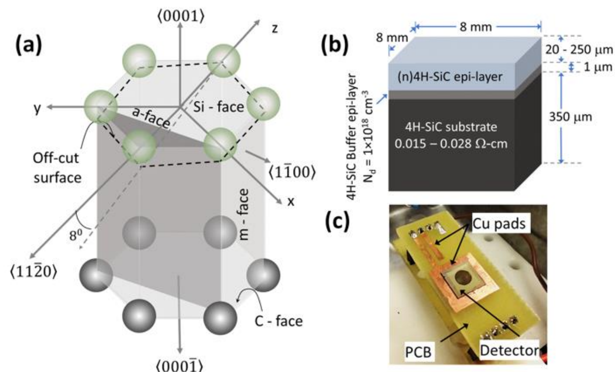

Fig. 1. Schematics showing the (a) crystal faces of 4H-SiC epilayers and (b) the substrate-epilayer configuration used for detector fabrication. (c) Photograph of a typical Ni/4H-SiC detector mounted on a PCB. The circular Ni Schottky and the square back contacts are also visible.

3 Device characterization

3.1 Electrical characterization

The performance of the SBDs depends on the material as well as the junction properties. The effective doping concentration of the epilayers used in this study is on the order of 10^{14} cm^{-3}, which is high enough to obscure the charge pairs ($\approx3\times10^{9}$ cm^{-3}) generated by incoming radiations. Hence, to generate a detector signal due to the motion of radiation induced charge pairs only, a detector active region is needed where the equilibrium carrier

concentration is orders of magnitude lower compared to the generated number of charge pairs. A Schottky barrier configuration is the most efficient and convenient way to generate a depletion region just underneath the contact surface, which is practically devoid of free carriers. Depending on the effective doping concentration of the 4H-SiC epilayer, depletion widths more than 100 µm can be achieved with a reverse bias of a few hundred volts. Puglisi *et al*. reported full depletion of a Schottky-type microstrip detector fabricated on a 124-µm thick 4H-SiC epilayer with a doping concentration of 5.2×10^{13} cm^{-3} at a bias voltage of 600 V [13]. The Schottky barrier height (SBH) restricts the leakage current flow under reverse bias which is important to reduce the electronic noise of the detector. Several refractory metals such as Ni, Ti, Pt, Re, W, Mo, and Ru form very stable Schottky contact which can withstand high temperatures normally encountered around RPVs and offer SBH over 1.5 eV ([22] and references therein). Apart from the current flow through the junction, charge carriers also flow on the surface which contributes to the total leakage current. Guard rings and/or passivated surfaces suppress the surface leakage current to a great extent. The current density J through the junction is mostly thermionic emission over a metal-semiconductor junction modelled as Eq. 1 [22].

$$J = A^{*}T^{2}\left(e^{-\beta\varphi_B}\right)\left(e^{\frac{\beta V}{n}} - 1\right), \tag{1}$$

where, $A*$ is the effective Richardson constant (146 Acm^{-2}K^{-2} for 4H-SiC), φ_B is the SBH, n is the diode ideality factor, V is the applied voltage, and $\beta = q/k_BT$, q being the electronic charge, k_B the Boltzmann constant, and T the absolute temperature. A $\ln J - V$ plot, V being the applied bias, is generated from the experimentally measured leakage current as a function of V. The SBH and the ideality factor are calculated from the intercept and slope of a linear fit of Eq. 1 to the $\ln J$- V plot[22]. Fig. 2(a) shows a $\ln J$- V plot in forward and reverse bias obtained for a Ni/20µm-4H-SiC SBD without a guard ring measured at room temperature using a Keithley 237 source-measure unit. The barrier height and the ideality factor were calculated to be 1.6 eV and 1.09, respectively. An ideality factor close to unity indicates that the barrier height is distributed uniformly across the contact area. Defects on the surface creates patches with low barrier heights through which a larger fraction of the total current may flow making the effective SBH lower [23]. The effective SBH and ideality factor also improves at high temperatures where the charge carriers acquire higher energy to overcome the higher SBH in the areas outside the low barrier patches [24]. The leakage current and ideality factor obtained for a similar but thicker Ni/150µm-4H-SiC SBD showed an improvement of the ideality factor from 1.9 at 350 K to 1.1 at 600 K with a corresponding increase in the SBH from 1.5 to 2.1 eV [16].

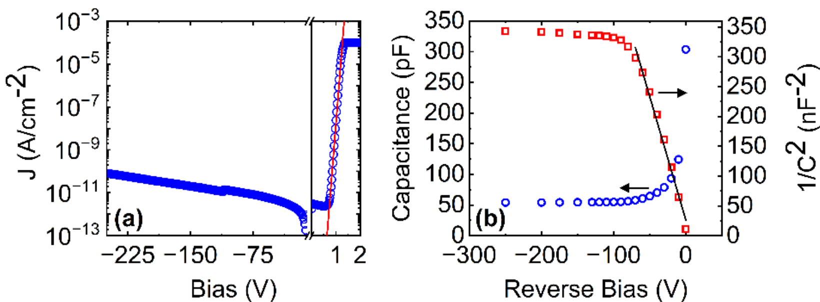

Fig. 2. (a) Semilogarithmic plot of current density as a function of forward and reverse bias for a Ni/20µm-4H-SiC SBD. The solid line is a linear fit of Eq. (1) to the forward lnJ-V plot. (b) Variation of detector capacitance (left y-axis) measured at 1 MHz test frequency as a function of reverse bias voltage and the corresponding Mott-Schottky plot (right y-axis).

Normally, the selection of the operating bias of radiation detectors is a trade-off between the leakage current and the charge collection efficiency (CCE). While it is essential to create an electric field high enough to ensure the collection of all the generated charge carriers, high fields can generate high leakage currents which increases the electronic noise. The Ni/4H-SiC detectors, however, allow 100% CCE and/or full depletion without substantial increase in the detector leakage current given the high barrier height and low effective doping concentration. The doping concentration is derived from the Mott-Schottky plots of the capacitance-voltage (C-V) characteristics at high measurement frequency [15]. Fig. 2(b) shows a C-V plot and the corresponding Mott-Schottky plot obtained for a Ni/20μm-4H-SiC SBD measured at a test frequency of 1 MHz. The operating bias voltage is usually set as the minimum bias at which the maximum CCE is observed. Further fine tuning of the bias is done to achieve the best resolution and will be discussed in Section 3.2.

3.2 Radiation detection

Alpha particle radiation detection measurements were carried out with a standard benchtop radiation spectrometer comprised of an Amptek A250CF preamplifier, an Ortec 576 shaping amplifier, a Canberra Multiport II MCA, and Genie 2000 - a PC based data acquisition program [15]. The detectors are exposed to a 1 μCi ^{241}Am radioisotope emitting primarily alpha particles with three energies *viz*., 5486, 5442, and 5388 keV. The detector and the source were kept inside a noise-shielded test box, which was continuously evacuated during the measurements. The detector was biased using a low noise Canberra 3106D power supply. Fig. 3(a) shows the variation of energy resolution and CCE of a Ni/20μm-4H-SiC SBD with reverse bias, calculated for the 5486 keV peak. The energy resolution is defined as the full width at half maximum (FWHM) in keV units or as the percentage of the peak energy. The CCE is defined as the ratio of the energy detected by the detector to the energy incident on the detector. It is usually calculated by the ratio of the alpha peak position in the calibrated spectrum to the incident alpha energy which in this case is 5486 keV. The observed initial improvement in the detector resolution with bias is due to the decrease in detector capacitance [9]. The CCE also increased initially as expected, and saturated to 100% at around -70 V. The best resolution was however obtained for -90 V with a shaping time of 3 μsec. The shaping time is optimized to obtain the highest peak resolution for the optimized bias. The recorded pulse height spectrum under the optimised setting is shown in Fig. 3(b). All the three primary alpha particles emitted by the source were fully resolved. The FWHM of the 5486 keV peak was measured to be 16.2 keV or 0.29% [9]. The energy resolution is comparable to the silicon SBD available commercially.

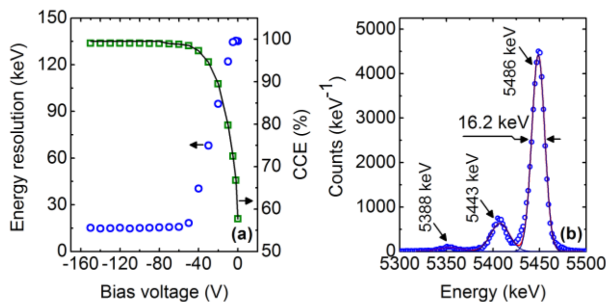

Fig. 3. (a) Variation of energy resolution (blue circles, left axis) and CCE (green squares, right axis) with reverse bias. The solid line shows the fitting of Eq. 2 to the measured CCE values. (b) Pulse height spectrum obtained using a Ni/20μm-4H-SiC SBD exposed to a ^{241}Am alpha source. The solid lines are the Gaussian fits.

3.3 Minority carrier diffusion length

The charge transport in a fully depleted detector, where all the radiation generated charge pairs are produced within the depletion region, is governed by the majority carriers. However, there are situations when the interactions occur beyond the depletion region (neutral region). In such cases the minority carriers (holes in the present n-type detectors) diffuse to the edge of the depletion region followed by a drift across the depletion width. The CCE in such a case is defined by the minority carrier transport (diffusion). A longer minority carrier diffusion length in such cases helps to achieve a 100% CCE even though the electrons are not collected. Such a situation is common for partially depleted detectors exposed to penetrating radiations such as during self-biased operations. Self-biased detectors are highly suitable for dosimetric applications where the logistics of locating a bias supply in or close to a high-temperature or high-radiation environment may by problematic [25]. Eq. 2 is a drift-diffusion model which expresses the variation of CCE (η) as a function of the detector bias (depletion width d) [26]. The solid line in Fig. 3(a) is a least square fitting of Eq. 2 to the variation of CCE with the bias voltage. The minority carrier diffusion length L_d was used as a fitting parameter and was found to be ~18 μm which is high enough to explain the 56% CCE at 0 V applied bias.

$$\eta = \frac{1}{E_p}\int_0^d \left(\frac{dE}{dx}\right) dx + \frac{1}{E_p}\int_d^{x_r} \left[\left(\frac{dE}{dx}\right) \times exp\left\{-\frac{(x-d)}{L_d}\right\}\right] dx \qquad (2)$$

where, dE/dx is the electronic stopping power of the alpha particles calculated using SRIM 2018 for several energies up to the one needed by the alpha particles to penetrate a depth d inside the detector, and x_r is the range of the alpha particles with energy E_p[27].

4 Neutron irradiation effects

In the above discussions, the performance of the best 4H-SiC detectors has been dealt with. Although, ultra-low leakage currents and 100% CCE are routinely achieved using these detectors, the energy resolution of the detectors is still far from the theoretical limits. This is primarily due to the presence of electrically active point defects in the as-grown epilayers which act as charge trapping centers. A detailed study on the correlation between the role of point defects and detector performance can be found in Ref. [28]. It is only obvious that with the accumulation of radiation dose in a reactor environment, over a prolonged period of use of the detectors, new types of trapping centers evolve as well as the concentration of the intrinsic trap centers increases. The effects of fast neutron irradiation on 250 μm thick 4H-SiC epilayers at four different neutron fluences have been studied [29]. Ni/4H-SiC SBDs were fabricated following the irradiation. The epilayers were irradiated in a TRIGA Mk. II nuclear reactor dry instrumentation tube at Kansas State University at net neutron fluences of $5 \times (10^{10}, 10^{11}, 10^{12}, \text{and } 10^{13})$ cm^{-2} in addition to background gamma doses varying from 400 Rad – 300 kRad linearly with the neutron fluence. Fig. 4(a)-(d) shows the changes in the detector performance with increases in neutron fluence. The energy peaks corresponding to the 5486 keV alpha particles have shifted left with increased neutron fluence. With the increase in the neutron fluence it is likely that a detector has accumulated higher concentration of newer as well as the existing defects. These defects, increased in concentration, participate in increased trapping of the radiation induced charge pairs leading to increased charge loss. The peak position in the pulse height spectrum, being directly proportional to the number of charges collected by the detector, shifts to a lower channel number with increased concentration of charge trapping centers. The deterioration of the energy resolution with increasing neutron fluence is clearly visible as the lower energy (5443

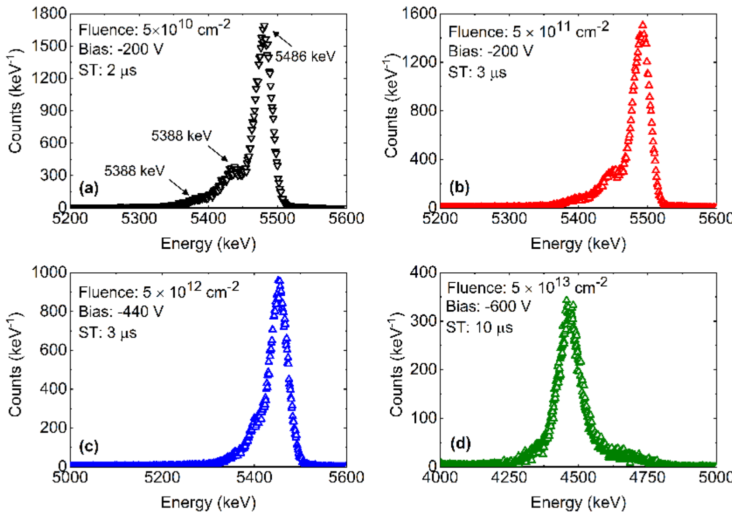

Fig. 4. (a)-(d) Pulse height spectra obtained for a Ni/250µm-4H-SiC SBD exposed to a ^{241}Am alpha source and irradiated with different neutron fluences.

and 5388 keV) alpha peaks gradually became unresolvable. Although the detectors with the first two doses showed similar energy resolution of ≈0.5% for the 5486 keV peak at -200 V, the one irradiated with higher fluence needed a larger shaping time of 3 µsec compared to the 2 µsec corresponding to the detector irradiated at the lowest dose. The increase in the optimum shaping time indicates increased trapping in the defects. Fig. 5(a) shows the

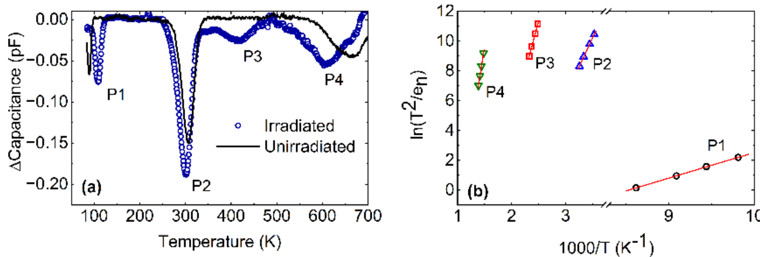

Fig. 5. (e) C-DLTS spectrum obtained for an unirradiated (solid line) the detector irradiated to a neutron fluence of 5 × 10^{11} cm^{-2} (open circles). (f) Arrhenius plots corresponding to the four trap centers observed in the C-DLTS spectra of the irradiated detector.

capacitance mode deep level transient spectra (C-DLTS) of an unirradiated SBD and an irradiated SBD to a neutron fluence of 5 × 10^{11} cm^{-2} obtained using a Sula Technologies DDS-12 deep level transient spectrometer. For the C-DLTS measurements, the diode was biased at a steady-state reverse bias voltage of -12 V. Filling pulses of height 0 V with a width of 2 msec and a period of 5 msec to 1 sec (depending on the rate window setting) were used. Fig. 5(b) shows the Arrhenius plots corresponding to each peak (trap center) from which the activation energies and the capture cross-sections were calculated. Peaks P1and P2 correspond to the Ti(c) impurity and $Z_{1/2}$ centers, which are commonly found in as-grown 4H-SiC [15]. The trap center corresponding to peak P3 is located 1.16 eV below the

conduction band minimum (CBM) and is identified as the CAV center [30]. The trap center corresponding to peak P4 is located 1.8 eV below the CBM and could not be identified. Both the trap centers corresponding to P3 and P4 are generally not observed in our as grown 4H-SiC layers and are supposedly created by the neutron irradiation at a fluence of 5×10^{11} cm^{-2}. Although with the increased neutron dosage the optimum bias and the shaping times increased, the CCE decreased, and the effective carrier concentrations decreased to a point transforming the SBD irradiated with the highest fluence to an Ohmic-like detector, the detector was still found to be functional with a moderately high energy resolution of 1.8% for alpha particles incident with 5486 keV energy.

5. Conclusions

The prospect of high-purity and low-defect 4H-SiC epilayers as radiation detectors has been investigated in this article for nuclear reactor dosimetric applications where conventional semiconductor detectors cannot function due to the high radiation background and temperatures. N-type 4H-SiC epitaxial layers with thickness in the range 20 – 250 μm with effective doping concentration on the order of 10^{14} cm^{-3} showed excellent rectification behaviour with very low reverse leakage currents ideal for high resolution radiation detectors. Ni/20μm-4H-SiC SBDs have demonstrated alpha particle detection with excellent energy resolution comparable to that of silicon detectors. Ni/250μm-4H-SiC SBDs irradiated with fast neutrons revealed that the detectors were functional with moderately high resolution even after a neutron fluence of 5×10^{13} cm^{-2}. The effect of the native and radiation-induced defects on the detector performance have been investigated using C-DLTS measurements. The C-DLTS measurements revealed the formation of new types of defects after irradiating the detectors with a neutron fluence of 5×10^{11} cm^{-2}. The capacitance or the junction properties for the higher fluences changed in a way where C-DLTS measurements could no longer be used to characterize the defects. Future work includes alternate defect characterization strategies to detect and identify the defects in these detectors. Also, theoretical calculations are underway to identify the new defects detected in the C-DLTS measurements.

The authors would like to thank Prof. Douglas S. McGregor and Daniel LP Watson of Kansas State University for use of the neutron irradiation facility. One of the authors (KCM) acknowledges the partial financial support obtained from the Department of Energy, Office of Nuclear Energy's Nuclear Energy University Programs (NEUP), Grant No. DE-NE0008662.

References

1. J. Guidez, J. Bodi, K. Mikityuk, E. Giardi, J. Bittan, B. A. Grah, H. Tsige-Tamirat, P. Romojaro, F. Álvarez-Velarde, B. Carluec, ASME J. Nucl. Rad. Sci. **8**, 011312 (2022).
2. N. Almirall, P. B. Wells, S. Pal, P. D. Edmondson, T. Yamamoto, K. Murakami, G. R. Odette, Scr. Mater. **181**, 134 (2020).
3. R. Vuiart, M. Brovchenko, J. Taforeau, V. Jaiswal, E. Drumonteil, Nucl. Sci. Eng. **196**, 455 (2021).
4. S. K. Chaudhuri and K. C. Mandal, "Radiation Detection Using n-Type 4H-SiC Epitaxial Layer Surface Barrier Detectors," in Iniewski K.. (eds) Advanced Materials for Radiation Detection, Cham., Springer, Chapter 9, pp. 183-209 (2022).
5. P. G. Neudeck, D. J. Spry, L. Chen, N. F. Prokop, M. J. Krasowski, IEEE Electron. Dev. Lett. **38**, 1082 (2017).

6. P. G. Neudeck, D. J. Spry, M. J. Krasowski, N. F. Prokop, L. Chen, Mater. Sci. Forum **963**, 813 (2019).
7. K. C. Mandal, J. W. Kleppinger, S. K. Chaudhuri, Micromachines **11**, 254 (2020).
8. F. H. Ruddy, L. Ottaviani, A. Lyoussi, C. Destouches, O. Palais, C. Reynard-Carette, IEEE Trans. Nucl. Sci. **69**, 792 (2022).
9. S. K. Chaudhuri, K. J. Zavalla, K. C. Mandal, Nucl. Instrum. Method Phys. Res. A **728**, 97 (2013).
10. F. H. Ruddy, A. R. Dulloo, J. G. Seidel, M. K. Das, R. Sei-Huang, A. K. Agarwal, IEEE Trans. Nucl. Sci. **53**, 1666 (2006).
11. C. S. Bodie, G. Lioliou, A. M. Barnett, Nucl. Instrum. Meth. Phys. Res. A **985**, 164663 (2021).
12. K. C. Mandal, P. G. Muzykov, S. K. Chaudhuri, J. Russell Terry, IEEE Trans. Nucl. Sci. **60**, 2888 (2013).
13. D. Puglisi and G. Bertuccio, Micromachines **10**, 835 (2019).
14. J. Coutinho, V. J. Torres, I. Capan, T. Brodar, Z. Ereš, R. Bernat, V. Radulović, K. Ambrožič, L. Snoj, Ž. Pastuović, A. Sarbutt, T. Ohshima, Y. Yamazaki, T. Makino, Nucl. Instrum. Meth, Phy. Res. A **986**, 164793 (2021).
15. S. K. Chaudhuri, J. W. Kleppinger, K. C. Mandal, J. Appl. Phys. **128**, 114501 (2020).
16. J. W. Kleppinger, S. K. Chaudhuri, O. Karadavut, K. C. Mandal, Appl. Phys. Lett. **119**, 063502 (2021).
17. J. W. Kleppinger, S. K. Chaudhuri, O. Karadavut, K. C. Mandal, J. Appl. Phys. **129**, 244501 (2021).
18. J. W. Kleppinger, S. K. Chaudhuri, O. F. Karadavut, R. Nag, K. C. Mandal, J. Cryst. Growth **583**, 126532 (2022).
19. J. J. Sumakeris, J. R. Jenny, A. R. Powell, MRS Bull. **30**, 280 (2011).
20. W. Kern, J. Electrochem. Soc. **137**, 1887 (1990).
21. S. K. Chaudhuri, K. J. Zavalla, K. C. Mandal, Appl. Phys. Lett. **102**, 031109 (2013).
22. Shalish and Y. Shapira, IEEE Elctron. Dev. Lett. **21**, 581 (2000).
23. S. M. Sze and K. K. Ng, *Physics of Semiconductor Devices*, (John Wiley & Sons, New Jersey, 2007).
24. R. T. Tung, Appl. Phys. Rev. **1**, 011304 (2014).
25. S. Seshadri, A. R. Dulloo, F. H. Ruddy, J. G. Seidel, L. B. Rowland, IEEE Trans. Electron Dev. **46**, 567 (1999).
26. M. B. H. Breese, J. Appl. Phys. **74**, 3789 (1993).
27. J. F. Ziegler, M. D. Ziegler, J. P. Biersack, Nucl. Instrum. Meth. Phys. Res. B **268**, 11, 1818 (2010).
28. K. C. Mandal, S. K. Chaudhuri, K. V. Nguyen, M. A. Mannan, IEEE Trans. Nucl. Sci. **61**, 2338 (2014).
29. J. W. Kleppinger, S. K. Chaudhuri, O. Karadavut, R. Nag, D. L. Watson, D. S. McGregor, K. C. Mandal, IEEE Trans. Nucl. Sci. Early Access, Apr. 2022.
30. N. T. Son, P. Stenberg, V. Jokubavicius, H. Abe, T. Ohshima, J. U. Hassan, I. G. Ivanov, Appl. Phys. Lett. **114**, 212105 (2019).